Expression and Regulation of Soluble Epoxide Hydrolase in Adipose Tissue

Bart M. De Taeye[1], Christophe Morisseau[2], Julie Coyle[1], Joseph W. Covington[1], Ayala Luria[2], Jun Yang[2], Sheila B. Murphy[1], David B. Friedman[3], Bruce B. Hammock[2] and Douglas E. Vaughan[1]

Obesity is an increasingly important public health issue reaching epidemic proportions. Visceral obesity has been defined as an important element of the metabolic syndrome and expansion of the visceral fat mass has been shown to contribute to the development of insulin resistance and cardiovascular disease. To identify novel contributors to cardiovascular and metabolic abnormalities in obesity, we analyzed the adipose proteome and identified soluble epoxide hydrolase (sEH) in the epididymal fat pad from C57BL/6J mice that received either a regular diet or a "western diet." sEH was synthesized in adipocytes and expression levels increased upon differentiation of 3T3-L1 preadipocytes. Although normalized sEH mRNA and protein levels did not differ in the fat pads from mice receiving a regular or a "western diet," total adipose sEH activity was higher in the obese mice, even after normalization for body weight. Furthermore, peroxisome proliferator–activated receptor γ (PPARγ) agonists increased the expression of sEH in mature 3T3-L1 adipocytes *in vitro* and in adipose tissue *in vivo*. Considering the established role for sEH in inflammation, cardiovascular diseases, and lipid metabolism, and the suggested involvement of sEH in the development of type 2 diabetes, our study has identified adipose sEH as a potential novel therapeutic target that might affect the development of metabolic and cardiovascular abnormalities in obesity.

Obesity (2010) **18,** 489–498. doi:10.1038/oby.2009.227

INTRODUCTION

Obesity, a chronic inflammatory condition, is an increasingly important public health issue reaching epidemic proportions (1). Visceral obesity has been defined as an important element of the metabolic syndrome and expansion of the visceral fat mass coupled with a disturbed metabolic profile has been shown to contribute to the development of insulin resistance and cardiovascular diseases (2,3). Understanding the (patho) physiological processes underlying the development of adipose tissue and the origin of markers associated with the development of type 2 diabetes, cardiovascular diseases, and chronic inflammation will help to identify new therapeutic candidates for the treatment or prevention of obesity development and obesity-associated disorders.

In order to identify novel factors that might contribute to the cardiovascular consequences of obesity, we performed a proteomic analysis of the epididymal fat pad from C57BL/6J mice that received either a regular diet or a "western diet" for 20 weeks. Soluble epoxide hydrolase (sEH), a cytosolic enzyme highly expressed in liver and kidney (4–6), was identified. Previous studies have established the relationship between sEH expression and hypertension (6–10). In addition, sEH has been related to increased inflammation (11–15) and a role in fatty acid and cholesterol metabolism has been suggested (16,17). A recent study identified a possible link between sEH and the development of diabetes (18).

Endogenous substrates for sEH include epoxy fatty acids such as epoxyeicosatrienoic acids or EETs. EETs are arachidonic acid metabolites produced by cytochrome P-450 epoxygenases (CYP450) (19) that produce a number of diverse actions in a variety of tissues and cells (reviewed in ref. 20). The conversion of EETs to dihydroxyeicosatrienoic acids (DHETs) by sEH forms the main catabolic pathway for EETs (reviewed in ref. 20). The mechanisms through which EETs exert their effects remain uncertain. While evidence supports a putative EET membrane receptor, data also support an intracellular mechanism in part by binding of EETs to a variety of intracellular proteins (reviewed in ref. 20). As such, it has been shown that EETs bind to peroxisome proliferator–activated receptor γ (PPARγ) and increase the PPARγ transcription activity in endothelial cells and 3T3-L1 preadipocytes (21) resulting in an anti-inflammatory response (22).

Considering the relevance of sEH for inflammation, cardiovascular disorders, and potentially insulin resistance/type 2

[1]Feinberg Cardiovascular Research Institute, Feinberg School of Medicine, Northwestern University, Chicago, Illinois, USA; [2]Department of Entomology and Cancer Research Center, University of California, Davis, California, USA; [3]Mass Spectrometry Research Center, Department of Biochemistry, Vanderbilt University, Nashville, Tennessee, USA. Correspondence: Bart M. De Taeye (b-taeye@northwestern.edu)

Received 29 May 2008; accepted 16 June 2009; published online 30 July 2009. doi:10.1038/oby.2009.227

diabetes, expression and regulation in adipose tissues and adipocytes were investigated. Our data indicate that sEH is expressed in adipocytes, expression increases during adipogenesis and is specifically induced in adipose tissue by PPARγ agonists.

METHODS AND PROCEDURES

Animals for proteomic analysis

Adult (6-week-old) male C57BL/6J mice were purchased from the Jackson Laboratory (Bar Harbor, ME). Mice were housed in a pathogen-free barrier facility (12 h light/12 h dark cycle). For the proteomic analysis, five animals received a regular, standard fat diet (SFD) for 20 weeks (diet 5001; LabDiet, Richmond, IN) in which 12% of the calories were derived from fat and five animals received a high-fat diet (HFD) for 20 weeks (diet TD 88137; Harlan Teklad, Madison, WI) in which 42% of total calories were derived from fat. Mice were weighed every 2 weeks. At the beginning and the end of the feeding period, body composition was determined using a Minispec model mq 7.5 (7.5 mHz) (Bruker Optics, Billerica, MA) and the animals were killed under anesthesia with isoflurane (Baxter, Deerfield, IL). The epididymal fat pads, livers, and kidneys were harvested and weighed; one part of the tissues was snap-frozen in liquid nitrogen and stored at −80 °C for further analysis while another part was fixed in 10% formalin for immunohistochemistry. To evaluate expression of sEH in different adipose depots, 6-week-old C57BL/6J mice were fed the HFD or SFD for 13 weeks; epididymal fat pads, subcutaneous fat pads, perirenal fat pads, and pericardial fat pads were collected and stored at −80 °C. These studies were initiated at the Vanderbilt University and completed at the Northwestern University. All animal protocols were approved by the Vanderbilt University Institutional Animal Care and Use Committee and the Northwestern University Institutional Animal Care and Use Committee.

Protein extraction

Protein was isolated from epididymal adipose tissue, liver, and kidney (200–400 mg). For proteomic analysis and western blotting, the samples were homogenized on ice in 1 ml lysis buffer (20 mmol/l HEPES, 50 mmol/l NaCl, 10% glycerol, 1% Triton-X 100, pH 7.4) in the presence of protease inhibitor cocktail (Complete Mini, Roche Diagnostics, Indianapolis, IN). After incubation for 1 h at 4 °C, samples were centrifuged at 4 °C for 20 min at 13,000 rpm. The aqueous layer containing the protein was collected. For the sEH activity assay, epididymal fat, liver, and kidney samples were homogenized in 3 ml of chilled 0.1 mol/l sodium phosphate buffer pH 7.4, containing 1 mmol/l EDTA, phenylmethylsulfonyl fluoride, and DTT; the homogenate was centrifuged at 11,000 rpm for 20 min at 4 °C; the supernatant solution was used as the enzyme extract. The extracts were snap-frozen in liquid nitrogen and stored at −80 °C until used. For each extraction method, protein concentration was determined using a bicinchoninic acid assay following the manufacturer's instructions (Pierce, Rockford, IL).

Analysis of the adipose proteome

Differences in protein levels were analyzed using proteomics technology, as described earlier (23). Protein samples (n = 3) were Cy-dye labeled using either Cy3 or Cy5 so that samples from each condition (SFD vs. HFD) received each labeling procedure to exclude a potential effect of labeling efficiency. A mix of all six samples was labeled using Cy2. Subsequently, 2D gel electrophoresis was performed using a pH 4–7 immobilized pH gradient. Three gels were run each containing a Cy3- and Cy5-labeled sample so that each gel contained a sample from both the SFD and HFD group. Each of the three gels also contained the Cy2-labeled mixture as internal standard. The Cy2, Cy3, and Cy5 components of each gel were individually imaged using mutually exclusive excitation/emission wavelengths. Finally, the gels were incubated in Sypro Ruby to ensure accurate protein excision, as the molecular weight and hydrophobicity of the Cy-dyes can influence protein migration during sodium dodecyl sulfate–polyacrylamide gel electrophoresis. DeCyder software (GE Healthcare, Piscataway, NJ) was used for simultaneous comparison of abundance changes across all three gels. The DeCyder biological variation analysis module was then used to simultaneously match all nine protein-spot maps from the three gels, and using the Cy3:Cy2 and Cy5:Cy2 differential in-gel analysis ratios, calculate average abundance changes and Student's t-test P values for the variance of these ratios for each protein-pair. Fold abundance changes are reported, whereby a fold increase is calculated directly from the volume ratio, and the fold decrease = 1/volume ratio (see **Supplementary Table S1** online).

Proteins of interest were robotically excised, equilibrated with 100 mmol/l ammonium bicarbonate for 20 min and dehydrated with two 10-min incubations with 100% acetonitrile in a 96-well plate format using Ettan Spot Picker and Digester workstations (GE Healthcare). Dehydrated gel plugs were manually digested in-gel with 10 µl porcine-modified trypsin protease (Promega, Madison, WI) in 25 mmol/l ammonium bicarbonate for 2 h at 37 °C. Tryptic peptides were then extracted from the gel plugs in two cycles of 60% acetonitrile, 0.1% trifluoroacetic acid using the Ettan Digester workstation and dried by vacuum centrifugation. Peptides were reconstituted in 10 µl of 0.1% trifluoroacetic acid, and manually desalted/concentrated into 2 µl of 60% acetonitrile, 0.1% trifluoroacetic acid using C18 ZipTip pipette tips (Millipore, Billerica, MA). The eluate, 0.5 µl, was analyzed using MALDI-TOF and tandem TOF/TOF mass spectrometry using a Voyager 4700 (Applied Biosystems, Foster City, CA). Ions specific for each sample were used to interrogate murine sequences entered in the SWISS-PROT and NCBInr databases using the MASCOT (http://www.matrixscience.com) and ProFound (http://prowl.rockefeller.edu) database search algorithms, respectively. Protein identifications from MALDI-TOF peptide mass maps are based on the masses of the tryptic peptides. Tandem mass spectrometry (MALDI-TOF/TOF) was used to generate limited amino acid sequence information on selected ions if additional confirmation was required.

Real-time quantitative PCR and reverse transcriptase PCR

RNA isolation, reverse transcription, and real-time quantitative PCR (RT-QPCR) were performed as described previously (24), with the primer sequences given in **Supplementary Table S2** online.

Reverse transcriptase–PCR was performed on cDNA created as described earlier (24). PCR products were analyzed on a 1% agarose gel followed by ethidium bromide staining. Reaction conditions and primers used are described in the referenced papers.

Western blotting

Proteins were separated using NuPAGE 4–12% Bis–Tris gels (Invitrogen, Carlsbad, CA) and transferred to Immobilon-P membranes (Millipore). After blocking, protein immunoblot analysis was performed using the appropriate primary antibodies (rabbit antiserum against mouse sEH, 1:20,000 (from B.D.H. and C.M., University of California, Davis, CA), rabbit polyclonal antibody for β-actin, 1:5,000 (Abcam, Cambridge, MA), and rabbit polyclonal antibody for perilipin, 1:1,000 (Abcam)) followed by horseradish peroxidase–conjugated anti-rabbit IgG antibody (1:10,000) (Santa Cruz Biotechnology, Santa Cruz, CA). Detection was done using the ECL Plus kit following manufacturer's instructions (GE Healthcare or Bio-Rad, Hercules, CA). Recombinant mouse sEH (from B.D.H. and C.M.) was used as a positive control in preliminary experiments to validate the specificity of the rabbit antiserum against mouse sEH.

Analysis of sEH activity

sEH activity was determined in liver, kidney, and epididymal fat pad, as described earlier (25), using [^{3}H]*trans*-stilbene oxide (*t*-SO). A 5 mmol/l *t*-SO solution (10,000 cpm/µl) in ethanol was prepared with cold *t*-SO (Sigma-Aldrich, St Louis, MO) and [^{3}H]*t*-SO (American Radiolabeled Chemicals, St Louis, MO). One microliter of this 5 mmol/l solution was added to 100 µl tissue extract, diluted 50-, 20-, or 5-fold in 0.1 mol/l sodium phosphate buffer, pH 7.4, containing 0.1 mg/ml bovine serum

albumin for liver, kidney, and fat, respectively. After incubation at 30 °C for 10, 15, and 60 min for liver, kidney, and fat, respectively, the reaction was stopped by addition of 250 µl of isooctane or hexanol. These reagents extracted the remaining epoxide or epoxide and diol, respectively, from the aqueous phase, and the quantity of radioactive diol present in the aqueous phase was measured by liquid scintillation counting. Each assay was performed in triplicate.

Immunohistochemistry

Tissues for immunohistochemistry were fixed in 10% neutral, phosphate-buffered formalin for 24–48 h and paraffin embedded. Subsequently the paraffin embedded tissues were processed in 6-µm sections. sEH antigen was localized using rabbit anti-mouse sEH IgG fraction (1:2,000). For detection ready-to-use biotinylated secondary antibodies against rabbit IgGs were used in combination with ready-to-use streptavidin–HRP and 3-amino-9-ethylcarbazole (all from BioGenex, San Ramon, CA).

Separation of adipocytes and stromal cells from adipose tissue

Three lean, 6-week-old male C57BL/6J mice, fed an SFD were killed as described earlier and their epididymal fat pads were collected. In addition, part of the epididymal fat pads of four of the 6-week-old male C57BL/6J mice that were fed the above described HFD for 13 weeks was used. From each mouse 300–500 mg of fat was collected in Dulbecco's modified Eagle's medium containing 1% bovine serum albumin and minced into fine pieces. The adipose tissue was digested using type 2 collagenase (1 mg/ml; Worthington, Lakewood, NJ) for 2 h at room temperature. The digested tissue was filtered through a 100-µm cell strainer (BD Falcon; BD Biosciences, Bedford, MA) followed by centrifugation at 300 *g*. The infranatant (liquid phase under the floating adipocytes) was collected using a syringe with needle. Fat cells were washed three times with phosphate-buffered saline, followed by centrifugation and collection of infranatant. Stromal cells were isolated by centrifuging the infranatant at 2,000 *g*. Stromal cells were washed two times with phosphate-buffered saline. Total RNA was isolated from both fractions using Trizol reagent (Invitrogen) following manufacturer's instructions. Leptin, F4/80, and sEH mRNA levels were quantified using RT-QPCR.

Culture and differentiation of 3T3-L1 cells

3T3-L1 cells were purchased from American Type Culture Collection (Rockville, MD) and cultured in Dulbecco's modified Eagle's medium (1 mg/ml glucose) supplemented with 10% fetal bovine serum and antibiotic–antimycotic solution (standard medium) in 100-mm culture dishes. For differentiation to adipocytes, cells were cultured in the appropriate plates (6-well or 100-mm), and when confluent (day 0), the standard medium was changed to differentiation medium (Dulbecco's modified Eagle's medium (4.5 mg/ml glucose) supplemented with 10% fetal bovine serum and antibiotic–antimycotic solution additionally supplemented with 0.5 mmol/l isobutylmethylxanthine, 1.0 µmol/l dexamethasone, and 10 µg/ml insulin) (Sigma-Aldrich). The differentiation medium was changed at days 2 and 4. Differentiation was considered to be complete at day 7. At this time >95% of the cells had accumulated fat droplets as shown by Oil Red O staining (Sigma-Aldrich). Before treatment, cells were incubated for 24 h in serum-free standard medium containing 1% bovine serum albumin (starvation medium). Subsequently cells were treated with troglitazone (Sigma-Aldrich) in starvation medium at concentrations and for the time indicated for the different experiments. After treatment, cells were washed with phosphate-buffered saline and collected in Trizol (RNA analysis) (Invitrogen) or lysis buffer (protein analysis).

Oxylipin extraction and analysis of 3T3-L1 cells and cell culture medium

Samples stored at −80 °C were thawed at room temperature and spiked with 10 µl of 500 nmol/l surrogate solution (26) and antioxidant solution (BHT:EDTA, 17 mg/ml) and oxylipins were extracted by solid phase extraction. Prior to that, cell pellets were manually homogenized in guanidinium thiocyanate solution (4 mol/l; Invitrogen) to elute nucleic acids from samples. Solid phase extraction was performed with Waters Oasis HLB cartridges (Waters, Milford, MA) and the cartridges were washed with 6 ml of a 5% methanol/water solution containing 0.1% acetic acid. The analytes were eluted with 0.5 ml methanol followed by elution with 2 ml of ethyl acetate. The eluate was evaporated with 10 µl of a trap solution (30% glycerol in methanol) by vacuum centrifugation. Prior to analysis, analytes were reconstituted by adding 50 µl of 200 nmol/l internal standard solution as described previously (26) to quantify recovery of surrogate standards so that recovery of ≥70% was accepted for analysis. Blank samples were phosphate-buffered saline samples spiked with analytical surrogates and antioxidants for calculation of limit of detection. All extracted samples were quantified using HPLC-MS/MS as previously described (26). Epoxides and diol analytes were quantified using the internal standard method and seven-point calibration curve fit with 1/x weighted either linear or quadratic curves ($r^2 > 0.997$).

Treatment of animals with rosiglitazone

Ten adult (6-week-old) male C57BL/6J mice were purchased from the Jackson Laboratory. Mice were housed in a pathogen-free barrier facility (12 h light/12 h dark cycle). All animals received the HFD for 12 weeks (diet TD 88137; Harlan Teklad, Madison, WI). Mice were weighed every 4 weeks. After 12 weeks, blood was collected after a 6-h fast and plasma glucose levels were analyzed using the Accu-Chek glucose meter (Roche Diagnostics, Indianapolis, IN). Subsequently, mice were treated with rosiglitazone (10 mg/kg/day in 1% carboxymethylcellulose in water) or vehicle by gavaging for 10 days. On day 10, the animals were subjected to an intraperitoneal glucose tolerance test after a 16-h overnight fast. Plasma glucose levels were determined at 0, 15, 30, 60, and 120 min using an Accu-Chek glucose meter; at each time point 10 µl blood was collected in EDTA-coated tubes (Microvette CB300; Sarstedt, Newton, NC) for determination of insulin levels using an ELISA specific for mouse insulin (Alpco Diagnostics, Salem, NH). After the intraperitoneal glucose tolerance test, mice received a final treatment with rosiglitazone or vehicle (day 11) and were euthanized the next day (day 12) after a 6-h fast under anesthesia with isoflurane (Baxter). The epididymal fat pads, subcutaneous fat pads, liver, and kidneys were harvested and stored at −80 °C for further analysis. All animal protocols were approved by the Northwestern University Institutional Animal Care and Use Committee.

Statistical analysis

Results are expressed as mean ± s.e.m. Comparisons between groups were carried out by unpaired Student's *t*-test or one-way ANOVA followed by Bonferroni's post-test where appropriate. For repetitive measurements, two-way ANOVA was used. Statistical analysis was performed using GraphPad Prism 4 (GraphPad, San Diego, CA).

RESULTS

The adipose proteome—identification of sEH

We hypothesized that novel or previously unrecognized proteins are expressed in visceral fat that contribute to the cardiovascular consequences of obesity. Therefore, the adipose proteome isolated from epididymal fat pads from C57BL/6J animals fed an HFD or an SFD for 20 weeks was analyzed ($n = 3$). Although initial body weights did not differ ($P > 0.05$), the animals fed an HFD were significantly heavier than their lean counterparts at the end of the feeding period ($P < 0.001$; **Table 1** and **Supplementary Figure S1** online). This was reflected in the % total adipose tissue ($P = 0.003$; **Table 1**) and was in agreement with a sixfold higher epididymal fat pad weight in the HFD group ($P = 0.0003$; **Table 1**).

Table 1 Obesity parameters for C57BL/6J animals in the study

	SFD	HFD
Initial weight (g)	19.7 ± 0.6	20.5 ± 0.5
End weight (g)*	30.8 ± 1.1	41.1 ± 1.5
Total adipose tissue (%)*	8.7 ± 0.7	32.2 ± 1.1
Epididymal fat pad weight (g)*	0.45 ± 0.05	2.65 ± 0.19

Data are mean ± s.e.m.
SFD, standard fat diet; HFD, high-fat diet.
*$P < 0.01$; $n = 5$.

From ~1,500 resolved proteins, 19 differentially expressed proteins were identified (selection based on $P < 0.05$ or fold change ≥1.5 (see **Supplementary Table S1**)). Among proteins that are typically detected in proteomic experiments such as kininogen, apolipoprotein AI, and α_2-macroglobulin, sEH was selected for further investigation because of its established roles in fatty acid metabolism, hypertension, and inflammation. sEH protein levels were 1.8-fold higher in the epididymal fat pad isolated from mice that received an HFD vs. an SFD ($P > 0.05$). In order to further evaluate this difference, western blot analysis for sEH was performed on total protein extracted from the epididymal fat pads from the C57BL/6J mice that received either the HFD or SFD for 20 weeks ($n = 5$). Although sEH was easily detectable in the adipose tissue extracts, no difference in sEH protein levels was detected when normalized to β-actin (data not shown). Similarly, RT-QPCR revealed no difference in sEH mRNA levels in the epididymal fat pads (data not shown).

It has been established that sEH is expressed in a variety of other organs, with higher levels found in liver and kidney (4,5,27). RT-QPCR analysis of sEH mRNA levels in liver, kidney, and epididymal fat pad of animals fed an SFD or HFD indicated that expression levels differ significantly among organs, with liver>kidney>fat ($P < 0.0001$; **Figure 1a**). However, diet did not influence the sEH mRNA levels ($P > 0.05$ for each organ) (**Figure 1a**). To evaluate expression of sEH in different adipose tissue depots, sEH mRNA levels in epididymal fat were compared with those in subcutaneous, perirenal, and pericardial fat pads from C57BL/6J mice fed an HFD or an SFD for 13 weeks ($n = 5$) (**Table 2**). No differences were observed for sEH levels in the different fat depots in comparison with the epididymal fat depot when considering animals fed an HFD; for the animals fed an SFD, perirenal and pericardial sEH mRNA levels were, respectively, higher and lower than those in the epididymal fat pad. Diet only influenced the sEH mRNA levels in the perirenal fat pad (**Table 2**). Due to limited amounts of the different fat pads, further analysis focused on the epididymal fat depot.

Total adipose sEH activity is increased in obese mice

While normalized sEH mRNA and protein levels did not differ in the epididymal fat pad from lean vs. obese animals, a higher total adipose sEH activity was anticipated for the obese animals. sEH-specific activity was generally in agreement with sEH mRNA data (**Figure 1b**). Although specific activity differed among organs with liver>kidney>fat ($P < 0.0001$), an HFD did not influence the activity. However, when total sEH activity was calculated for each of the different organs and normalized for body weight, the HFD was associated with a 18% increase and a 42% decrease in liver ($P = 0.10$) and kidney ($P = 0.003$) sEH activity, respectively, whereas it increased total epididymal fat sEH activity by 138% ($P = 0.008$) (**Figure 1c**).

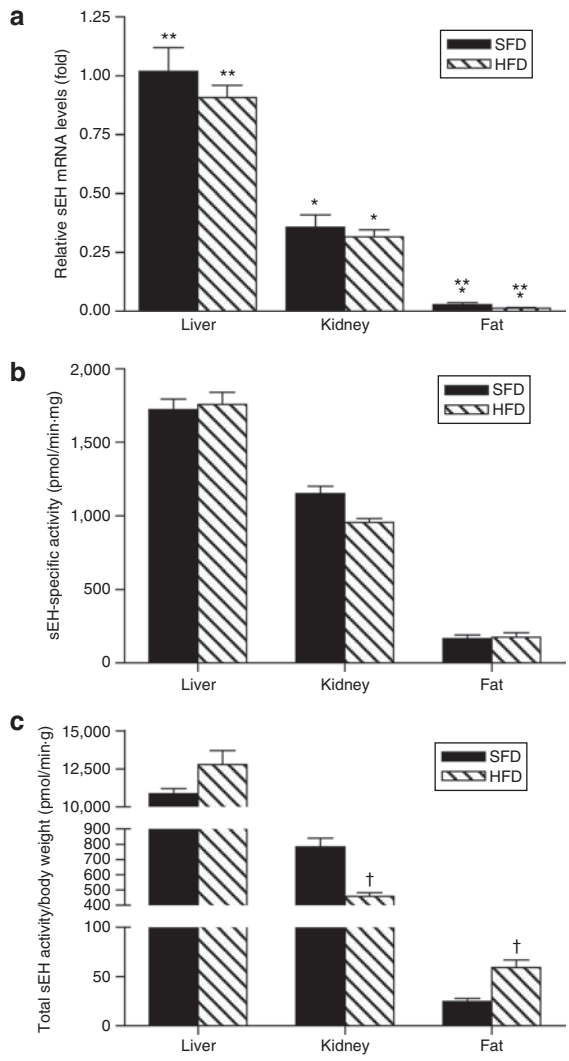

Figure 1 Tissue soluble epoxide hydrolase expression. (**a**) Soluble epoxide hydrolase (sEH) mRNA levels and (**b,c**) activity for liver, kidney, and epididymal fat pad. (**a**) All data are expressed relative to liver standard fat diet (SFD). Diet had no effect on sEH mRNA levels ($P > 0.05$ for each organ). (**b,c**) sEH activity is expressed per mg protein (**b**) and for the total organ after normalization for body weight (**c**). *$P < 0.001$ vs. liver for the same diet; **$P < 0.01$ vs. kidney for the same diet; †$P < 0.01$ vs. SFD. $n = 5$.

Adipocytes are a source of sEH

Adipose tissue consists of adipocytes and stromal cells such as endothelial cells and macrophages. Both endothelial cells and macrophages have been shown to express sEH (5,28,29). Immunohistochemical analysis of the epididymal fat pads from mice that received either an SFD or an HFD for 20 weeks

confirmed the presence of sEH in endothelial cells and macrophages in adipose tissue and suggested sEH production in adipocytes (**Supplementary Figure S2** online).

After separation of the adipocyte and stromal fractions from the freshly isolated epididymal fat pad from 6-week-old C57BL/6J mice fed an SFD, RT-QPCR analysis indicated that both fractions express sEH. In the adipocyte-enriched fraction, sEH mRNA levels were fourfold higher in comparison with the stromal fraction (4.03 ± 0.33 vs. 1.01 ± 0.08, P = 0.0009, relative to stromal fraction; n = 3 per group), indicating that adipocytes actually express sEH. Leptin mRNA and F4/80 mRNA levels were 3.57 ± 0.17- and 1.43 ± 0.06-fold higher in the adipocyte and stromal fractions, respectively, indicative for an enrichment of each fraction (P = 0.0002 and 0.04, respectively). The same analysis was performed on freshly isolated epididymal fat pads from C57BL/6J mice fed an HFD for 13 weeks; sEH mRNA levels were again fourfold higher in the adipocyte-enriched fraction in comparison with the stromal fraction (4.3 ± 0.19 vs. 1.05 ± 0.21, P < 0.0001, relative to stromal fraction; n = 4 per group). Leptin mRNA and F4/80 mRNA levels were 2.56 ± 0.23- and 1.83 ± 0.17-fold higher in the adipocyte and stromal fractions, respectively (P = 0.0005 and 0.005, respectively).

To further characterize sEH expression in adipocytes, 3T3-L1 cells were used in *in vitro* experiments. sEH was found to be expressed in 3T3-L1 preadipocytes and levels increased significantly upon differentiation into mature adipocytes (**Figure 2**). mRNA levels of sEH increased during a 7-day differentiation period (P < 0.0001), during which markers of adipogenesis showed an expected profile: fatty acid binding protein (aP2) mRNA increased and preadipocyte factor-1 mRNA decreased (P < 0.0001 for each; **Figure 2d**).

Table 2 Body weight and sEH mRNA levels in different fat pads

	SFD	HFD
Initial weight (g)	21.3 ± 0.5	21.1 ± 0.6
End weight (g)*	28.9 ± 0.6	42.6 ± 0.7
Epididymal fat	1.15 ± 0.30	0.54 ± 0.09
Subcutaneous fat	0.46 ± 0.07	0.77 ± 0.16
Perirenal fat*	2.14 ± 0.41†	0.78 ± 0.15
Pericardial fat	0.02 ± 0.004†	0.09 ± 0.04

Data are mean ± s.e.m.; n = 5. sEH mRNA levels are expressed relative to epididymal fat SFD.
sEH, soluble epoxide hydrolase; SFD, standard fat diet; HFD, high-fat diet.
*P < 0.001 for HFD vs. SFD, †P < 0.05 vs. epididymal fat.

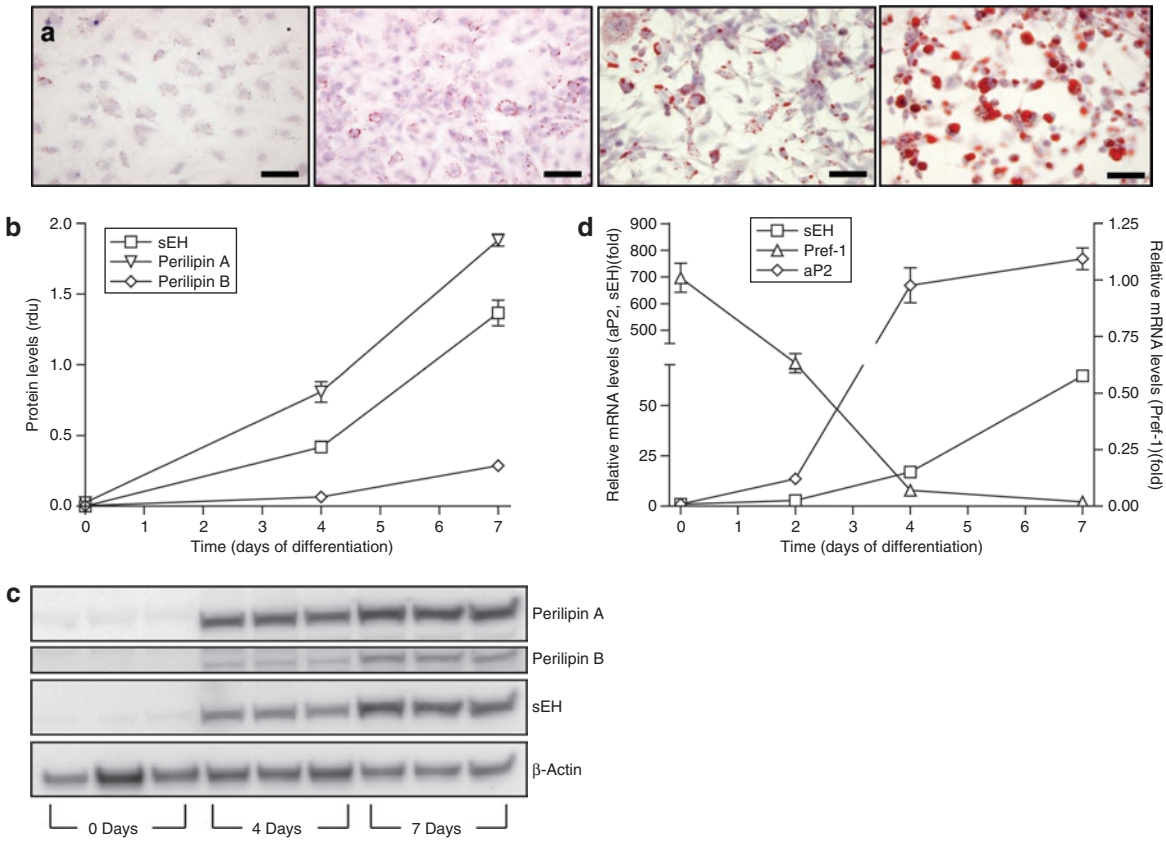

Figure 2 Soluble epoxide hydrolase (sEH) in 3T3-L1 cells. (**a**) Differentiation of 3T3-L1 preadipocytes was analyzed by Oil Red O staining at days 0, 2, 4, and 7 (left to right). Bar = 50 µm. Western blotting for perilipin A and B and sEH indicated that sEH protein levels increased during preadipocyte differentiation ((**b**), densitometric analysis (rdu, relative densitometric units); (**c**) representative bands for perilipin A, perilipin B, sEH, and control actin). n = 3. (**d**) aP2, sEH, and Pref-1 mRNA levels determined by real-time quantitative PCR indicated that sEH mRNA levels increased during preadipocyte differentiation. n = 6.

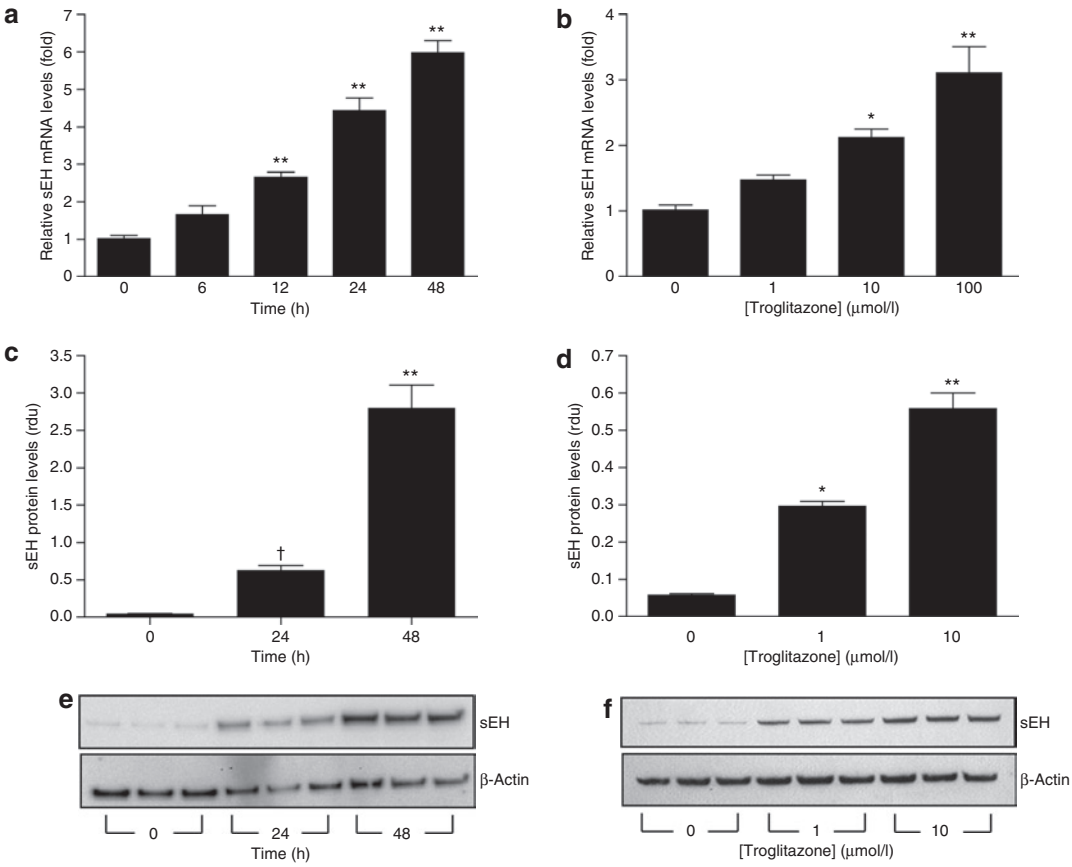

Figure 3 Troglitazone regulates soluble epoxide hydrolase (sEH) expression in mature 3T3-L1 adipocytes. (**a,b**) sEH mRNA levels in 3T3-L1 adipocytes determined by real-time quantitative PCR during incubation with troglitazone (**a**, 10 μmol/l; **b**, 48 h). $n = 6$. (**c–f**) Western blotting of sEH and control actin in 3T3-L1 adipocytes during incubation with troglitazone (**c**,**e**, 10 μmol/l; **d,f**, 48 h) (rdu, relative densitometric units). (**e,f**) Western blots used for quantitation in **c** and **d**, respectively. $n = 3$. $^{\dagger}P < 0.05$; $^{*}P < 0.01$; $^{**}P < 0.001$ vs. baseline.

Lipid accumulation was confirmed by Oil Red O staining (Figure 2a). sEH protein levels also increased significantly upon differentiation of 3T3-L1 preadipocytes ($P < 0.0001$; Figure 2b,c). The increase in perilipin A and B protein was in agreement with the gradual increase of lipid droplet formation ($P < 0.0001$ for both targets) (30).

In order to confirm that the sEH expression in adipocytes was biologically active, EET levels were systematically quantified. EET levels were significantly higher in preadipocytes than in mature adipocytes (**Supplementary Figure S3a** online). Whereas all four EET regioisomers were easily detectable in preadipocytes (day 0), by day 4 the levels had decreased significantly, often below the level of detection. EET levels in cell culture medium showed a profile similar as seen for intracellular EETs (**Supplementary Figure S3c**). Generally, levels of DHETs followed the same trend as EET levels (**Supplementary Figure S3b,d**).

To investigate whether CYP450 enzymes shown to produce the different EET regioisomers from arachidonic acid are present in adipose tissue and mature 3T3-L1 adipocytes, reverse transcriptase was used for various CYP2C's and CYP2J9 using primers and cycling conditions as described earlier (31–34). Interestingly, CYP2C55 and 2J9 were identified in both adipose tissue and mature 3T3-L1 adipocytes (**Supplementary Figure S4**).

PPARγ agonists induce sEH expression in mature 3T3-L1 adipocytes

The current study provides evidence that sEH levels increase during adipogenesis. To further examine this relationship, 3T3-L1 adipocytes were treated with troglitazone, a PPARγ agonist known to exert its effect by inducing and maintaining adipogenesis/lipogenesis (35,36). Treatment of differentiated 3T3-L1 cells with troglitazone resulted in a time-dependent increase in sEH mRNA (Figure 3a) and protein (Figure 3c,e). Furthermore, troglitazone exerted a concentration-dependent effect, increasing both sEH mRNA (Figure 3b) and protein levels (Figure 3d,f).

To investigate the effect of PPARγ agonists on sEH expression in adipose tissue *in vivo,* a diet-induced model of obesity/insulin resistance was used. Obese C57BL/6J mice were treated with 10 mg/kg/day rosiglitazone, a clinically used PPARγ agonist, or vehicle. Data showed that rosiglitazone improved insulin sensitivity associated with lower plasma insulin and glucose levels as described earlier (37) (**Supplementary Figures S5** and **S6** online). sEH mRNA levels and activity were significantly increased in the epididymal fat pad of mice receiving the PPARγ agonist (Figure 4a,b). Immunohistochemistry indicated that in agreement with mRNA, sEH protein levels were increased in the epididymal fat pad after rosiglitazone

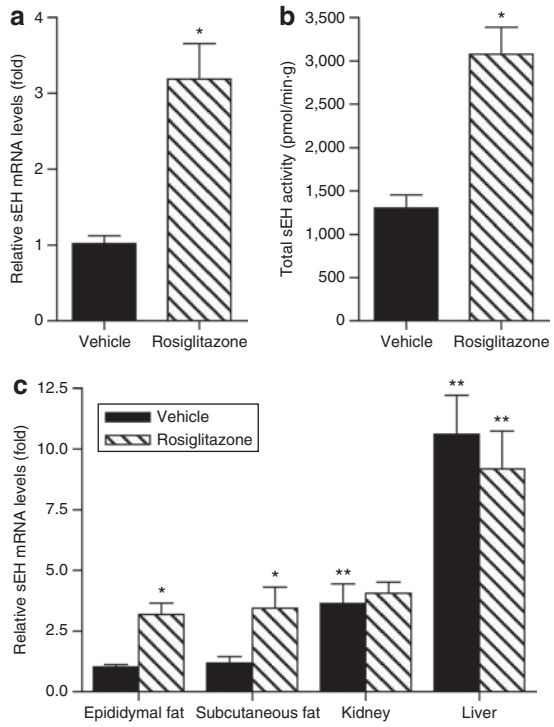

Figure 4 Rosiglitazone increases soluble epoxide hydrolase (sEH) expression in adipose tissue. (**a**) sEH mRNA levels and (**b**) activity were increased in the epididymal fat pad of obese C57BL/6J mice by rosiglitazone. (**c**) Rosiglitazone also increased sEH expression in subcutaneous fat whereas levels of kidney and liver sEH mRNA were not influenced. $n = 5$. $^{*}P < 0.05$ vs. vehicle; $^{**}P < 0.05$ vs. epididymal fat.

treatment (**Supplementary Figure S7**). Whereas sEH mRNA levels in the subcutaneous fat pad showed a profile similar to the epididymal fat pad levels ($P = 0.03$; **Figure 4c**), rosiglitazone did not influence liver or kidney sEH mRNA levels (**Figure 4c**). Interestingly, rosiglitazone-induced sEH mRNA levels in the epididymal and subcutaneous fat were similar to kidney sEH mRNA levels (**Figure 4c**).

DISCUSSION

The present study indicates that sEH is expressed and synthesized in 3T3-L1 cells and adipose tissue. Although the expression of sEH has been identified in numerous tissues, including the liver and kidney (4,5), to our knowledge there are no previous reports describing adipose tissue, or adipocytes more specifically, as a source of sEH. In addition, thiazolidinediones, a class of PPARγ agonists that stimulate adipogenesis/lipogenesis (35,36), increase expression levels of sEH in 3T3-L1 adipocytes *in vitro* and adipose tissue *in vivo*.

Although the current study does not directly link adipose sEH with inflammatory amplification in obesity, hypertension, or type 2 diabetes, the present findings serve to identify sEH as a potential contributor to these disorders. The goal of the study was to identify novel mechanistic or therapeutic candidates contributing to the cardiovascular consequences of obesity. Because sEH has been shown to contribute to angiotensin II–induced hypertension (7), left ventricular hypertrophy (38), and atherosclerosis (39), its increased production in adipocytes and visceral fat is potentially important. By deactivating EETs, sEH augments inflammation (15,21), which is known to contribute to local and systemic insulin resistance. By enhancing the bioavailability of EETs in obesity, sEH inhibition may provide a novel strategy to reduce inflammation (15). Furthermore, EETs have been shown to function as natural PPARγ ligands which may contribute to their anti-inflammatory effect (21). A recent study suggested a link between sEH and the development of diabetes (18), in agreement with the triad obesity–inflammation–insulin resistance.

Previous studies have established the relationship between sEH expression and hypertension (6–10,28,40). It remains to be established whether sEH derived from adipocytes influences vascular resistance locally or systemically. Adipose tissue comprises a substantial proportion of total body weight and it has been long recognized that an extensive capillary network surrounds adipose tissue (41). EETs have been shown to cause vasodilation by acting as autocrine or paracrine hormones (42). Increased levels of sEH in adipose tissue could lead to a decreased release of endogenous EETs and/or an increased clearance of exogenous EETs produced by other cell types in adipose tissue such as endothelial cells. Alternatively, the stimuli that promote sEH expression in fat may also induce increased sEH activity in vascular tissue remote from visceral fat. This possibility is currently under investigation.

Our data support a potential role for sEH in adipogenesis. Loss-of-function studies demonstrated that PPARγ plays a critical role in adipogenesis *in vivo* and *in vitro* (43,44). Ligand-activated PPARγ regulates many genes involved in glucose and lipid homeostasis and is therefore involved in the maintenance of normal insulin responsiveness (45). One of the questions remaining today with regard to PPARγ and adipogenesis is the identity of a possible endogenous ligand (46). Numerous reports have described a wide variety of structurally different molecules that the PPARγ ligand binding domain can accommodate in its large hydrophobic pocket (47). PPARγ ligands include the thiazolidinediones (48), polyunsaturated fatty acids (49), and arachidonic acid metabolites such as 15-deoxy-$\Delta^{12,14}$ prostaglandin J (50,51), among others. Other metabolites derived from arachidonic acid by either the lipoxygenase or cyclooxygenase have been shown to positively or negatively influence adipogenesis (52,53). With regard to the third pathway of arachidonic acid metabolism, the CYP450 epoxygenase pathway, only a limited number of studies have been performed. Madsen *et al.* reported that inhibition of the lipoxygenase, but not the cyclooxygenase or CYP450 epoxygenase pathway, prevents adipocyte differentiation in 3T3-L1 cells (54). Interestingly, however, Liu *et al.* showed that EETs, generated from arachidonic acid by CYP450 epoxygenases, can bind and activate PPARγ (21). In addition, it has been shown that EETs combined with an sEH inhibitor can induce the expression of aP2 in 3T3-L1 preadipocytes, indicative of adipocyte differentiation (21). Based on this prior observation and in combination with our data showing that EETs are present in preadipocytes and that sEH

is upregulated during adipogenesis, it can be hypothesized that EETs contribute to preadipocyte maturation by activating PPARγ. In this scenario, sEH could form a negative feedback mechanism to prevent further adipogenic signaling once the mature adipocyte phenotype has been established. In support of this, it has been shown that overexpression of sEH reduces PPARγ activity (21). The precise identity of the EETs involved in adipocyte differentiation is uncertain. Our data suggest that 5,6-EET might play an important role considering the higher levels in comparison with the other EETs. Higher levels of 5,6-EET are in agreement with the fact that sEH effectively hydrolyzes 8,9-, 11,12-, and 14,15-EET, whereas 5,6-EET is a poor substrate for sEH (20). This hypothesis is supported further by our finding of reduced 5,6-DHET levels in comparison with the other DHET regioisomers in the medium of undifferentiated 3T3-L1 cells. Finally, DHET levels decrease with differentiation, which can be explained by the lower levels of EETs available for hydration. Although lower levels of EETs in mature adipocytes suggest that CYP450 activity decreases upon differentiation of preadipocytes, additional studies are necessary. Interestingly, sEH inhibitors are currently being evaluated for their potential to treat insulin resistance. Based on our findings, sEH inhibitors should increase the levels of EETs in adipose tissue simulating treatment with PPARγ agonists. With regard to the hypothesized decreased activity of CYP450 in mature adipocytes, it remains to be investigated whether sEH inhibitors will be effective. Indeed, inhibiting sEH can preserve the potentially important low levels of EETs in mature adipocytes. Alternatively, considering the low EET levels, sEH inhibitors might have no effect. Further studies are necessary to investigate the effect of CYP450, EETs, and sEH on adipogenesis and insulin resistance/type 2 diabetes.

Intriguingly, considering the apparent role of sEH in inflammation, hypertension, and type 2 diabetes development, the data presented here showing that thiazolidinediones induce sEH *in vitro* and *in vivo* might seem counterintuitive. However, higher sEH levels may provide a negative feedback loop preventing further adipocyte differentiation. A tight *in vivo* regulation of sEH-mediated EET hydrolysis in adipose tissue can be anticipated based on the fact that EETs, acting as PPARγ ligands, indirectly induce their own hydrolysis via stimulation of sEH expression. Furthermore, EET-induced aP2 (21), which binds EETs, likely influences the metabolism, bioavailability, and activity of EETs (20). Further studies are necessary to investigate the complex interaction between the various components of the arachidonic acid/CYP450/EET/sEH pathway and PPARγ.

sEH expression in adipose tissue is significantly lower than that observed in liver and kidney. However, although the normalized concentration of sEH in fat did not increase when animals were fed an HFD, total adipose sEH activity was higher in obese vs. lean mice. Total adipose sEH activity was selectively increased during the development of obesity. Furthermore, rosiglitazone specifically induced sEH expression and activity in adipose tissue, resulting in levels similar to those in kidney. Thus, adipose tissue exhibits the greatest relative increase in sEH levels either due to consumption of a "western diet" or due to the use of PPARγ agonists. Of interest, the diet-induced increase in sEH activity seen for liver probably reflects activation of abundant liver PPARα, which has been shown to induce sEH expression (55). In this context, it is of interest to note that activation of the different members of the PPAR family can result in increased sEH expression. Why sEH levels decrease in kidney when animals are fed an HFD is not clear. Finally, in lean animals different levels of sEH mRNA were observed in perirenal and pericardial fat in comparison with epididymal and subcutaneous fat. Although this suggests fat depot specificity for sEH expression, further investigation is necessary. The limited amount of the described fat depots in lean mice prevents detailed analysis. With regard to the higher sEH mRNA levels in perirenal fat it cannot be excluded that during the collection of this depot some kidney cortex expressing sEH was co-collected.

Whether PPARγ agonists directly induce sEH expression cannot be concluded from the current study. It is feasible that PPARγ activates other transcription factors and/or induces lipogenic enzymes resulting in an increase in lipid signaling molecules that can induce sEH expression. Although increased levels of some DHETs formed after hydrolysis of EETs by sEH may retain biological activity (20), limited *in vivo* activity can be anticipated because DHETs are quite water soluble and rapidly conjugated. In addition, other epoxides are substrates for sEH (56). Considering the different functions of EETs and their metabolites and the different expression profiles between rodents and humans (7), the current results have to be interpreted with caution. Nevertheless, our study suggests that selective sEH inhibitors, which are currently under investigation to treat hypertension and insulin resistance, might be of value in treating metabolic and cardiovascular consequences of obesity.

In conclusion, our study is the first to report the expression of sEH in adipose tissue, and more specifically in the adipocyte itself. Data suggest that EETs can be considered as novel adipokines, whose bioavailability can be regulated by adipose sEH. Where previous studies have shown that EETs are PPARγ ligands, our data show that sEH expression is upregulated by PPARγ agonists suggesting a complex reciprocal autoregulatory mechanism. As such, sEH in adipose tissue is topologically and functionally poised to influence local inflammation, lipid metabolism, and adipogenesis. The (patho)physiological importance of sEH expression in adipose tissue and its regulation by PPARγ agonists merits further investigation for the role this plays in obesity and its comorbidities.

SUPPLEMENTARY MATERIAL

Supplementary material is linked to the online version of the paper at http://www.nature.com/oby

ACKNOWLEDGMENTS

This study was supported by the National Institutes of Health (NIH) grant SCCOR P50HL081089, a postdoctoral fellowship from the American Heart Association (0625319B), and partial support from the National Institute of Environmental Health Sciences R37 ES02710 and NIH HL85727.

DISCLOSURE

B.D.H. founded Arete Therapeutics (Hayward, CA; http://www.aretetherapeutics.com) to develop soluble epoxide hydrolase inhibitors for the treatment of high blood pressure, cardiovascular diseases, and type 2 diabetes.

REFERENCES

1. Smyth S, Heron A. Diabetes and obesity: the twin epidemics. *Nat Med* 2006;12:75–80.
2. Katagiri H, Yamada T, Oka Y. Adiposity and cardiovascular disorders: disturbance of the regulatory system consisting of humoral and neuronal signals. *Circ Res* 2007;101:27–39.
3. Poirier P, Giles TD, Bray GA *et al*. Obesity and cardiovascular disease: pathophysiology, evaluation, and effect of weight loss: an update of the 1997 American Heart Association Scientific Statement on Obesity and Heart Disease from the Obesity Committee of the Council on Nutrition, Physical Activity, and Metabolism. *Circulation* 2006;113:898–918.
4. Enayetallah AE, French RA, Thibodeau MS, Grant DF. Distribution of soluble epoxide hydrolase and of cytochrome P450 2C8, 2C9, and 2J2 in human tissues. *J Histochem Cytochem* 2004;52:447–454.
5. Yu Z, Davis BB, Morisseau C *et al*. Vascular localization of soluble epoxide hydrolase in the human kidney. *Am J Physiol Renal Physiol* 2004;286:F720–F726.
6. Sinal CJ, Miyata M, Tohkin M *et al*. Targeted disruption of soluble epoxide hydrolase reveals a role in blood pressure regulation. *J Biol Chem* 2000;275:40504–40510.
7. Jung O, Brandes RP, Kim IH *et al*. Soluble epoxide hydrolase is a main effector of angiotensin II-induced hypertension. *Hypertension* 2005;45:759–765.
8. Imig JD, Zhao X, Capdevila JH, Morisseau C, Hammock BD. Soluble epoxide hydrolase inhibition lowers arterial blood pressure in angiotensin II hypertension. *Hypertension* 2002;39:690–694.
9. Imig JD, Zhao X, Zaharis CZ *et al*. An orally active epoxide hydrolase inhibitor lowers blood pressure and provides renal protection in salt-sensitive hypertension. *Hypertension* 2005;46:975–981.
10. Yu Z, Xu F, Huse LM *et al*. Soluble epoxide hydrolase regulates hydrolysis of vasoactive epoxyeicosatrienoic acids. *Circ Res* 2000;87:992–998.
11. Node K, Huo Y, Ruan X *et al*. Anti-inflammatory properties of cytochrome P450 epoxygenase-derived eicosanoids. *Science* 1999;285:1276–1279.
12. Kozak W, Kluger MJ, Kozak A, Wachulec M, Dokladny K. Role of cytochrome P-450 in endogenous antipyresis. *Am J Physiol Regul Integr Comp Physiol* 2000;279:R455–R460.
13. Falck JR, Reddy LM, Reddy YK *et al*. 11,12-epoxyeicosatrienoic acid (11,12-EET): structural determinants for inhibition of TNF-alpha-induced VCAM-1 expression. *Bioorg Med Chem Lett* 2003;13:4011–4014.
14. Sasaki M, Ostanin D, Elrod JW *et al*. TNF-alpha -induced endothelial cell adhesion molecule expression is cytochrome P-450 monooxygenase dependent. *Am J Physiol, Cell Physiol* 2003;284:C422–C428.
15. Schmelzer KR, Kubala L, Newman JW *et al*. Soluble epoxide hydrolase is a therapeutic target for acute inflammation. *Proc Natl Acad Sci USA* 2005;102:9772–9777.
16. EnayetAllah AE, Luria A, Luo B *et al*. Opposite regulation of cholesterol levels by the phosphatase and hydrolase domains of soluble epoxide hydrolase. *J Biol Chem* 2008;283:36592–36598.
17. Newman JW, Morisseau C, Harris TR, Hammock BD. The soluble epoxide hydrolase encoded by EPXH2 is a bifunctional enzyme with novel lipid phosphate phosphatase activity. *Proc Natl Acad Sci USA* 2003;100:1558–1563.
18. Larsen BT, Campbell WB, Gutterman DD. Beyond vasodilatation: non-vasomotor roles of epoxyeicosatrienoic acids in the cardiovascular system. *Trends Pharmacol Sci* 2007;28:32–38.
19. Capdevila JH, Falck JR, Harris RC. Cytochrome P450 and arachidonic acid bioactivation. Molecular and functional properties of the arachidonate monooxygenase. *J Lipid Res* 2000;41:163–181.
20. Spector AA, Norris AW. Action of epoxyeicosatrienoic acids on cellular function. *Am J Physiol, Cell Physiol* 2007;292:C996–1012.
21. Liu Y, Zhang Y, Schmelzer K *et al*. The antiinflammatory effect of laminar flow: the role of PPARgamma, epoxyeicosatrienoic acids, and soluble epoxide hydrolase. *Proc Natl Acad Sci USA* 2005;102:16747–16752.
22. Pasceri V, Wu HD, Willerson JT, Yeh ET. Modulation of vascular inflammation *in vitro* and *in vivo* by peroxisome proliferator-activated receptor-gamma activators. *Circulation* 2000;101:235–238.
23. Friedman DB, Hill S, Keller JW *et al*. Proteome analysis of human colon cancer by two-dimensional difference gel electrophoresis and mass spectrometry. *Proteomics* 2004;4:793–811.
24. De Taeye BM, Novitskaya T, McGuinness OP *et al*. Macrophage TNF-alpha contributes to insulin resistance and hepatic steatosis in diet-induced obesity. *Am J Physiol Endocrinol Metab* 2007;293:E713–E725.
25. Morisseau C, Hammock, BD. Measurement of soluble epoxide hydrolase (sEH) activity. *Curr Protoc Toxicol* 2007;33:4.23.1–4.23.18.
26. Luria A, Weldon SM, Kabcenell AK *et al*. Compensatory mechanism for homeostatic blood pressure regulation in Ephx2 gene-disrupted mice. *J Biol Chem* 2007;282:2891–2898.
27. Pacifici GM, Temellini A, Giuliani L *et al*. Cytosolic epoxide hydrolase in humans: development and tissue distribution. *Arch Toxicol* 1988;62:254–257.
28. Rodriguez M, Clare-Salzler M. Eicosanoid imbalance in the NOD mouse is related to a dysregulation in soluble epoxide hydrolase and 15-PGDH expression. *Ann N Y Acad Sci* 2006;1079:130–134.
29. Ai D, Fu Y, Guo D *et al*. Angiotensin II up-regulates soluble epoxide hydrolase in vascular endothelium *in vitro* and *in vivo*. *Proc Natl Acad Sci USA* 2007;104:9018–9023.
30. Greenberg AS, Egan JJ, Wek SA *et al*. Isolation of cDNAs for perilipins A and B: sequence and expression of lipid droplet-associated proteins of adipocytes. *Proc Natl Acad Sci USA* 1993;90:12035–12039.
31. Wang H, Zhao Y, Bradbury JA *et al*. Cloning, expression, and characterization of three new mouse cytochrome p450 enzymes and partial characterization of their fatty acid oxidation activities. *Mol Pharmacol* 2004;65:1148–1158.
32. Tsao CC, Foley J, Coulter SJ *et al*. CYP2C40, a unique arachidonic acid 16-hydroxylase, is the major CYP2C in murine intestinal tract. *Mol Pharmacol* 2000;58:279–287.
33. Qu W, Bradbury JA, Tsao CC *et al*. Cytochrome P450 CYP2J9, a new mouse arachidonic acid omega-1 hydroxylase predominantly expressed in brain. *J Biol Chem* 2001;276:25467–25479.
34. DeLozier TC, Tsao CC, Coulter SJ *et al*. CYP2C44, a new murine CYP2C that metabolizes arachidonic acid to unique stereospecific products. *J Pharmacol Exp Ther* 2004;310:845–854.
35. Tamori Y, Masugi J, Nishino N, Kasuga M. Role of peroxisome proliferator-activated receptor-gamma in maintenance of the characteristics of mature 3T3-L1 adipocytes. *Diabetes* 2002;51:2045–2055.
36. Hamm JK, el Jack AK, Pilch PF, Farmer SR. Role of PPAR gamma in regulating adipocyte differentiation and insulin-responsive glucose uptake. *Ann N Y Acad Sci* 1999;892:134–145.
37. Liu LF, Purushotham A, Wendel AA, Belury MA. Combined effects of rosiglitazone and conjugated linoleic acid on adiposity, insulin sensitivity, and hepatic steatosis in high-fat-fed mice. *Am J Physiol Gastrointest Liver Physiol* 2007;292:G1671–G1682.
38. Ai D, Pang W, Li N *et al*. Soluble epoxide hydrolase plays an essential role in angiotensin II-induced cardiac hypertrophy. *Proc Natl Acad Sci USA* 2009;106:564–569.
39. Ulu A, Davis BB, Tsai HJ *et al*. Soluble epoxide hydrolase inhibitors reduce the development of atherosclerosis in apolipoprotein e-knockout mouse model. *J Cardiovasc Pharmacol* 2008;52:314–323.
40. Fleming I. DiscrEET regulators of homeostasis: epoxyeicosatrienoic acids, cytochrome P450 epoxygenases and vascular inflammation. *Trends Pharmacol Sci* 2007;28:448–452.
41. Crandall DL, Hausman GJ, Kral JG. A review of the microcirculation of adipose tissue: anatomic, metabolic, and angiogenic perspectives. *Microcirculation* 1997;4:211–232.
42. Spector AA, Fang X, Snyder GD, Weintraub NL. Epoxyeicosatrienoic acids (EETs): metabolism and biochemical function. *Prog Lipid Res* 2004;43:55–90.
43. Kubota N, Terauchi Y, Miki H *et al*. PPAR gamma mediates high-fat diet-induced adipocyte hypertrophy and insulin resistance. *Mol Cell* 1999;4:597–609.
44. Rosen ED, Sarraf P, Troy AE *et al*. PPAR gamma is required for the differentiation of adipose tissue *in vivo* and *in vitro*. *Mol Cell* 1999;4:611–617.
45. Walczak R, Tontonoz P. PPARadigms and PPARadoxes: expanding roles for PPARgamma in the control of lipid metabolism. *J Lipid Res* 2002;43:177–186.

46. Tontonoz P, Spiegelman BM. Fat and beyond: the diverse biology of PPARgamma. *Annu Rev Biochem* 2008;77:289–312.
47. Nolte RT, Wisely GB, Westin S *et al*. Ligand binding and co-activator assembly of the peroxisome proliferator-activated receptor-gamma. *Nature* 1998;395:137–143.
48. Murphy GJ, Holder JC. PPAR-gamma agonists: therapeutic role in diabetes, inflammation and cancer. *Trends Pharmacol Sci* 2000;21:469–474.
49. Hertzel AV, Bernlohr DA. Regulation of adipocyte gene expression by polyunsaturated fatty acids. *Mol Cell Biochem* 1998;188:33–39.
50. Forman BM, Tontonoz P, Chen J *et al*. 15-Deoxy-delta 12, 14-prostaglandin J2 is a ligand for the adipocyte determination factor PPAR gamma. *Cell* 1995;83:803–812.
51. Kliewer SA, Lenhard JM, Willson TM *et al*. A prostaglandin J2 metabolite binds peroxisome proliferator-activated receptor gamma and promotes adipocyte differentiation. *Cell* 1995;83:813–819.
52. Xie Y, Kang X, Ackerman WE *et al*. Differentiation-dependent regulation of the cyclooxygenase cascade during adipogenesis suggests a complex role for prostaglandins. *Diabetes Obes Metab* 2006;8:83–93.
53. Yan H, Kermouni A, Abdel-Hafez M, Lau DC. Role of cyclooxygenases COX-1 and COX-2 in modulating adipogenesis in 3T3-L1 cells. *J Lipid Res* 2003;44:424–429.
54. Madsen L, Petersen RK, Sørensen MB *et al*. Adipocyte differentiation of 3T3-L1 preadipocytes is dependent on lipoxygenase activity during the initial stages of the differentiation process. *Biochem J* 2003;375:539–549.
55. Pinot F, Grant DF, Spearow JL, Parker AG, Hammock BD. Differential regulation of soluble epoxide hydrolase by clofibrate and sexual hormones in the liver and kidneys of mice. *Biochem Pharmacol* 1995;50:501–508.
56. Greene JF, Williamson KC, Newman JW, Morisseau C, Hammock BD. Metabolism of monoepoxides of methyl linoleate: bioactivation and detoxification. *Arch Biochem Biophys* 2000;376:420–432.

Supplementary Table 1. DIGE and Mass Spectrometry and Database Search Results

DIGE analysis using DeCyder 2D v6.5
MS acquisition/processing: 4000 Explorer Series v3.0 (2000 laser shots per PMF, 2000 per ms/ms)
S/N<3 peak filtering, local noise window width = 250, min. peak width at FWHM = 2.9, without baseline correction or smoothing.
database searching: GPS Explorer v3.6 running the MASCOT v1.9 suite of database search algorithms. Searches performed at 200 ppm peptide mass accuracy without constraining
database: Sprot20070410 (283454 sequences; 104030551 residues).

		Protein Table T-test and Av.Ratio: WT SFD / WT HFD									
Pos.	Master No.	T-test[1]	WT SFD / WT HFD Av. Ratio[2]	Acc. Num	MW, pI[3]	MOWSE[4]	Protein Identification	Peptide	ppm	ms/ms score	Modification
1	525	0.038	-1.55	FTHFD_MOUSE	99.5 kDa, 5.6 pI	149,23,3,31%	10-formyltetrahydrofolate D				
2	536	0.042	-1.68				10-formyltetrahydrofolate D				
								GRLLYR	-72		
								ADPLGLEAEKDGVPVFK	-11		
								ILPNVPEVEDSTDFFK	-10		
								GSASSALELTEEELATAEAVR	-9		
								LFVEDSIHDQFVQK	-8		
								FLFPEGIK	-6		
								HGSIIYHPSLLPR	-6		
								GVVNILPGSGSLVGQR	-6	4	
								DTNHGPQNHEAHLR	-6		
								TDVAAPFGGFK	-5		
								EESFGPIMIISR	-5		Oxidation (M)[8]
								ANATEFGLASGVFTR	-5		
								RPQPEEGATYEGIQKK	-5		
								FADGDVDAVLSR	-4	13	
								IQGATIPINQARPNR	-4		
								LQAGTVFVNTYNK	-3		
								RPQPEEGATYEGIQK	-3		
								DLGEAALNEYLR	-1		
								AGLILFGNDDR	1	14	
								THVGMSIQTFR	1		Oxidation (M)[5]
								MMPASQFFK	2		Oxidation (M)[1,2]
								ECDVLPDDTVSTLYNR	11		Carbamidomethyl (C)[2]
								LIAEGTAPR	20		
3	905	0.012	1.68	KNG1_MOUSE	74 kDa, 6.0 pI	140,9,4,14%	kininogen				
4	906	7.30E-05	1.93				kininogen				
								DIPVDSPELK	-14		
								ENEFFIVTQTCK	-4	23	Carbamidomethyl (C)[11]
								EVLGHSIAQLNAENDHPFYYK	9		
								GNLFMDINNK	-3		Oxidation (M)[5]
								QFNPGVK	-5		
								RPPGFSPFR	-2	24	
								SGNQYMLHR	-1		Oxidation (M)[6]
								TDGSPTFYSFK	-6	27	
								YVIEFIAR	2	38	
5	918	0.028	-2.01	PLSL_MOUSE	70.7 kDa, 5.2 pI	231,13,6,23%	L-plastin / Plastin-2				
								AYYHLLEQVAPK	-11		
								FSLVGIAGQDLNEGNR	-4	47	
								GDEEGIPAVVIDMSGLR	-2	3	Oxidation (M)[13]
								IGLFADIELSR	-3		
								ISFDEFIK	-4	29	
								LSPEELLLR	0	35	

Protein Table T-test and Av.Ratio: WT SFD / WT HFD

Pos.	Master No.	T-test[1]	WT SFD / WT HFD Av. Ratio[2]	Acc. Num	MW, pI[3]	MOWSE[4]	Protein Identification	Peptide	ppm	ms/ms score	Modification
								MINLSVPDTIDER	-4		Oxidation (M)[1]
								NEALIALLR	2	20	
								QFVTATDVVR	-6	45	
								VNKPPYPK	-4		
								VYALPEDLVEVNPK	-8		
								YAISMAR	-9		Oxidation (M)[5]
								YTLNILEDIGGGQK	-14		
6	978	0.18	-1.5	LKHA4_MOUSE	69.6 kDa, 5.9 pI	111,16,2,28%	leukotrine-A4-hydrolase				
								APLPLGHIK	-2	11	
								ASMHPVTAMLVGR	-6		Oxidation (M)[3,9]
								DVDPDVAYSSIPYEK	-3	19	
								ELVALMSAIR	1		Oxidation (M)[6]
								FTRPLFK	-2		
								GSPMEISLPIALSK	-10		Oxidation (M)[4]
								MKFTRPLFK	-1		Oxidation (M)[1]
								MQEVYNFNAINNSEIR	0		Oxidation (M)[1]
								SANEFSETESMLK	-3		Oxidation (M)[11]
								SFLYSHFK	-3		
								SHDQAVHTYQEHK	-2		
								TFGESHPFTK	-3		
								TLTGTAALTVQSQEENLR	-2		
								TQHLHLR	0		
								VVINGQEVK	-14		
								YTLGESQGYK	-5		
7	1023	0.0052	1.7	PGM1_MOUSE	61.7 kDa, 6.3 pI	169,20,2,42%	phosphoglucomutase				
								ADNFEYSDPVDGSISK	-4		
								DLEALMLDR	9		Oxidation (M)[6]
								ELLSGPNR	-6		
								FFGNLMDASK	0		Oxidation (M)[6]
								FKPFTVEIVDSVEAYATMLR	-26		Oxidation (M)[18]
								FNISNGGPAPEAITDK	-11		
								FYMTEAIQLIVR	-5		Oxidation (M)[3]
								IDAMHGVVGPYVK	-7		Oxidation (M)[4]
								LIFADGSR	-2		
								LSGTGSAGATIR	8		
								NIFDFNALK	-6		
								QEATLVVGGDGR	1		
								QQFDLENK	-4		
								SGEHDFGAAFDGDGDR	-1		
								SGEHDFGAAFDGDGDRNMILGK	6		Oxidation (M)[18]
								SMPTSGALDRVANATK	-13		Oxidation (M)[2]
								TIEEYAICPDLKVDLGVLGK	-33		Carbamidomethyl (C)[8]
								TQAYPDQKPGTSGLR	-4	14	
								VSQLQER	6		
								YDYEEVEAEGANK	-7	22	
8	1085	0.0078	1.41	CH60_MOUSE			60 kDa HSP				
9	1098	0.0051	1.51		61 kDa, 5.9 pI	242,15,7,31%	60 kDa HSP				
								AAVEEGIVLGGGCALLR	-2		Carbamidomethyl (C)[13]
								APGFGDNR	1	9	
								APGFGDNRK	3		
								FGADAR	8	6	
								GANPVEIR	-5	15	
								GYISPYFINTSK	-3	38	

Pos.	Master No.	Protein Table T-test[1]	T-test and Av.Ratio: WT SFD / WT HFD WT SFD / WT HFD Av. Ratio[2]	Acc. Num	MW, pI[3]	MOWSE[4]	Protein Identification	Peptide	ppm	ms/ms score	Modification
								IGIEIIKR	4	8	
								IQEITEQLDITTSEYEKEK	7		
								ISSVQSIVPALEIANAHR	-3	8	
								KPLVIIAEDVDGEALSTLVLNR	-4		
								LKVGLQVVAVK	1		
								LVQDVANNTNEEAGDGTTTATVL/	5	79	
								TLNDELEIIEGMKFDR	1		Oxidation (M)[12]
								VGLQVVAVK	-6		
								VTDALNATR	5		
10	1121	0.11	-1.82	HYES_MOUSE	63 kDa, 5.8 pI	146,10,4,22%	soluble epoxide hydrolase				
								AKPNEVVFLDDFGSNLKPAR	-2	11	
								ATEIGGILVNTPEDPNLSK	3	65	
								AVASLNTPFMPPDPDVSPMK	8		Oxidation (M)[10,19]
								DIVLRPEMSK	0		Oxidation (M)[8]
								DMGMVTILVHNTASALR	3		Oxidation (M)[2,4]
								RSEEALALPR	-8		
								SEEALALPR	-2		
								SINRPMLQAAIALK	-4	3	Oxidation (M)[6]
								SINRPMLQAAIALKK	2		Oxidation (M)[6]
								YQIPALAQAGFR	-2	30	
11	1214	0.0029	2.36	TBA1A_MOUSE	50.7 kDa, 4.9 pI	45,10,0,32%	alpha-tubulin				
								AVFVDLEPTVIDEVR	-7		
								EDAANNYAR	-4		
								EIIDLVLDR	-2		
								FDGALNVDLTEFQTNLVPYPR	1		
								IHFPLATYAPVISAEK	-2		
								LIGQIVSSITASLR	-2		
								NLDIERPTYTNLNR	-7		
								QLFHPEQLITGK	-4		
								TIGGGDDSFNTFFSETGAGK	-3		
								VGINYQPPTVVPGGDLAK	3		
12	1445	0.013	-2.25	GUAD_MOUSE	51.5 kDa, 5.4 pI	155,15,3,33%	guanine deaminase				
								AVMVSNVLLINK	-2		Oxidation (M)[3]
								EFDALLINPR	0		
								FLYLGDDR	0	10	
								FLYLGDDRNIEEVYVGGK	5		
								FVSEMLQK	-15		Oxidation (M)[5]
								IGLGTDVAGGYSYSMLDAIR	1		Oxidation (M)[15]
								IVFLEESSQQEK	-7	20	
								NIEEVYVGGK	-7		
								NYTDVYDKNNLLTNK	-2		
								RAVMVSNVLLINK	-9		Oxidation (M)[4]
								STDVAEEVYTR	-6		
								THDLYIQSHISENREEIEAVK	3		
								TPPLALVFR	0	23	
								VKPIVTPR	-1		
								YTFPTEQR	-1		
13	1463	0.024	-1.44	ENOA_MOUSE	47.4 kDa, 6.4 pI	271,15,7,42%	alpha enolase				
14	1470	0.015	-1.65				alpha enolase				
								AAVPSGASTGIYEALELR	-1	26	
								AGYTDQVVIGMDVAASEFYR	7		Oxidation (M)[11]
								DATNVGDEGGFAPNILENK	9	17	
								EIFDSR	5	7	

Protein Table T-test and Av.Ratio: WT SFD / WT HFD

Pos.	Master No.	T-test[1]	WT SFD / WT HFD Av. Ratio[2]	Acc. Num	MW, pI[3]	MOWSE[4]	Protein Identification	Peptide	ppm	ms/ms score	Modification
								FTASAGIQVVGDDLTVTNPK	1	25	
								GNPTVEVDLYTAK	1	50	
								GVSQAVEHINK	2		
								IDKLMIEMDGTENK	14		Oxidation (M)[5,8]
								IGAEVYHNLK	0		
								LAMQEFMILPVGASSFR	4		Oxidation (M)[3,7]
								SFRNPLAK	8		
								SGKYDLDFK	13		
								YDLDFK	-4		
								YITPDQLADLYK	1	44	
								YNQILR	6	7	
15	1816	0.025	2.16	A2M_MOUSE	167 kDa, 6.2 pI	157,14,8,10%	alpha2 macroglobulin (fragment)				
								APFALQVNTLPLNFDK	4	20	
								EVLVTIESSGTFSK	2	22	
								GSGSGCVYLQTSLK	14		Carbamidomethyl (C)[6]
								KLQDQPNIQR	-3		
								LLLQEVR	7		
								LPDLPGNYVTK	-1	28	
								LQDQPNIQR	-1	11	
								MVSGFIPMKPSVK	-3	2	Oxidation (M)[1,8]
								NLKPAPIK	1		
								QQNSHGGFSSTQDTVVALQALSK	8		
								TEVNTNHVLIYIEK	-2	32	
								TFHVNSGNR	-1		
								YGAATFTR	2	7	
								YNILPVADGK	1	7	
16	1940	0.039	-1.5	ANXA5_MOUSE	35.7 kDa, 4.8 pI	470,22,9,69%	ANX5				
17	1944	0.013	-1.47				ANX5				
								ADAEVLR	-2		
								ADAEVLRK	-1		
								DLVDDLKSELTGK	-8		
								ETSGNLEQLLLAVVK	-45		
								FITIFGTR	5	29	
								GAGTDDHTLIR	-2	8	
								GLGTDEDSILNLLTSR	-5		
								GTVTDFPGFDGR	-1	34	
								KNFATSLYSMIK	-1		Oxidation (M)[10]
								LIVAMMKPSR	-2		Oxidation (M)[5,6]
								LYDAYELK	-6	26	
								MLVVLLQANR	-2		Oxidation (M)[1]
								NFATSLYSMIK	-6	56	Oxidation (M)[9]
								QEIAQEFK	-6	16	
								QVYEEEYGSNLEDDVVGDTSGYY	13	48	
								SEIDLFNIR	1	33	
								SEIDLFNIRK	3		
								SIPAYLAETLYYAMK	-2		Oxidation (M)[14]
								TPEELSAIK	-6		
								VLTEIIASR	2	16	
								WGTDEEK	132		
								YMTISGFQIEETIDR	-3		Oxidation (M)[2]
18	2089	0.0046	-1.64				actin fragment				
								DLYANTVLSGGTTMYPGIADR	-4	1	Oxidation (M)[14]
								EKMTQIMFETFNTR	17		

Protein Table T-test and Av.Ratio: WT SFD / WT HFD

Pos.	Master No.	T-test[1]	WT SFD / WT HFD Av. Ratio[2]	Acc. Num	MW, pI[3]	MOWSE[4]	Protein Identification	Peptide	ppm	ms/ms score	Modification
								GYSFTTTAER	0	10	
								IIAPPER	2		
								IIAPPERK	6		
								SYELPDGQVITIGNER	-6	44	
								VAPEEHPVLLTEAPLNPK	-8		
19	2179	0.014	-1.58				actin fragment				
								FLYANTVLSGGSTMFPGIADR	-6		Oxidation (M)[14]
								IIAPPER	9		
								IIAPPERK	-1		
								QEYDESGPSIVHR	-4		
								SYELPDGQVITIGNER	-8	48	
20	2216	0.021	-1.13	PRDX6_MOUSE	24.9 kDa, 5.7 pI	102,10,4,48%	peroxiredoxin 6				
								DFTPVCTTELGR	-2		Carbamidomethyl (C)[6]
								IRFHDFLGDSWGILFSHPR	3		
								KGESVMVVPTLSEEEAK	-10		Oxidation (M)[6]
								LPFPIIDDK	-9	4	
								LPFPIIDDKGR	-4	10	
								LSILYPATTGR	-3		
								NFDEILR	1		
								PGGLLLGDEAPNFEANTTIGR	-5	3	
								VVFIFGPDK	-3		
								VVFIFGPDKK	-5	16	
21	2222	0.0034	-2.18	TPIS_MOUSE	27 kDa, 6.9 pI	36,4,2,17%	triosephosphate isomerase				
								HVFGESDELIGQK	-2	19	
								RHVFGESDELIGQK	-5		
								TATPQQAQEVHEK	-11		
								VTNGAFTGEISPGMIK	-6	2	Oxidation (M)[14]
22	2235	0.0004	1.55	APOA1_MOUSE			apolipoprotein AI				
23	2247	0.059	1.11		30.5 kDa, 5.6 pI	371,15,7,39%	apolipoprotein AI				
								ARPALEDLR	-2	33	
								DFANVYVDAVK	-6	63	
								ESLAQR	6		
								LGPLTR	10		
								LQELQGR	14	22	
								LSPVAEEFR	2	31	
								LSPVAEEFRDR	-5	15	
								QEMNK	-177		Oxidation (M)[3]
								QKLQELQGR	-1		
								SNPTLNEYHTR	-5		
								TQLAPHSEQMR	-3		Oxidation (M)[10]
								VAPLGAELQESAR	-4	58	
								VKDFANVYVDAVK	-11		
								VQPYLDEFQK	-6	28	
								VQPYLDEFQKK	-13		
24	2306	0.0033	-1.56	KCY_MOUSE	22.3 kDa, 5.7 pI	90,8,3,54%	UMP-CMP kinase				
								FLIDGFPR	1	11	
								IQTYLESTKPIIDLYEEMGK	-11		Oxidation (M)[18]
								IVPVEITISLLKR	-4		
								KNPDSQYGELIEK	-3		
								MKPLVVFVLGGPGAGK	-5	7	Oxidation (M)[1]
								REMDQTMAANAQK	37		
								SVDEVFGEVVK	2	14	
								YGYTHLSAGELLR	-1		

Protein Table T-test and Av.Ratio: WT SFD / WT HFD

Pos.	Master No.	T-test[1]	WT SFD / WT HFD Av. Ratio[2]	Acc. Num	MW, pI[3]	MOWSE[4]	Protein Identification	Peptide	ppm	ms/ms score	Modification
25	2455	0.038	2.33	CYB5_MOUSE	15.2 kDa, 4.9 pI	61,3,2,34%	cytochrome b5				
								EQAGGDATENFEDVGHSTDAR	-43		
								FLEEHPGGEEVLR	-54	15	
								TYIIGELHPDDR	-54	29	
26	2525	0.0014	-1.67	LEG1_MOUSE	15.2 kDa, 5.3 pI	248,7,4,54%	galectin1				
								DSNNLCLHFNPR	-1		Carbamidomethyl (C)[6]
								FNAHGDANTIVCNTK	-4		Carbamidomethyl (C)[12]
								LNMEAINYMAADGDFK	-3		Oxidation (M)[3,9]
								LNMEAINYMAADGDFK	-3	55	Oxidation (M)[3,9]
								LPDGHEFK	-4	58	
								LPDGHEFKFPNR	-7		
								SFVLNLGK	-4	52	
								VRGEVASDAK	-2	29	

[1,2] average volume ratios and Student's t-test p-values were calculated using DeCyder software version 6.5 without FDR correction, utilizing the mixed-sample internal standard methodology as described in materials and methods.

[3] MW and pI values are derived from database entries. For proteins present in the database as precursor forms, the reported values may not accurately reflect the MW and pI position of the mature protein analyzed here.

[4] MOWSE=A, B(x), C, D are MOWSE combined MS and MS/MS search scores, number of peptides matched (number of unmatched peptides), number of peptides with MS/MS data, and percent of the amino acids accounted for by the matching peptides (coverage). Molecular Weight Search (MOWSE) scores above 67 are within the 95th percentile confidence interval, but additional information such as gel position and correspondance with known site-specific cleavages for peptide ms/ms were also considered.

Supplementary table 2 Real-time quantitative PCR primers

Target	Primer sequence 5’ to 3’
sEH sense	CCATAAGTCAAATATTCAGCCAAG
sEH antisense	TATCAGGAAGTCAAAGTGTTGG
aP2 sense	GCGTGGAATTCGATGAAATCA
aP2 antisense	CCCGCCATCTAGGGTTATGA
Pref-1 sense	AATAGACGTTCGGGCTTGCA
Pref-1 antisense	GGAGCATTCGTACTGGCCTTT
Leptin sense	CCCCTCAGATCCTCCAAAAT
Leptin antisense	AACCCTGCTTGCAGTCTATT
F4/80 sense	TTTCCTCGCCTGCTTCTTC
F4/80 antisense	CCCCGTCTCTGTATTCAACC
β-actin sense	GATTACTGCTCTGGCTCCTAGCA
β-actin antisense	GCCACCGATCCACACAGAGT

Supplementary Figures and Legends

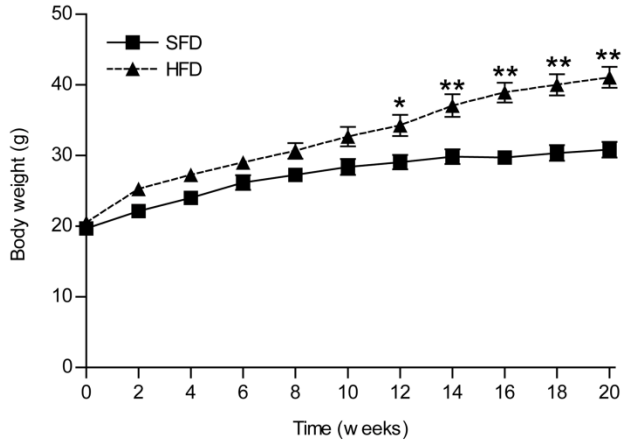

Supplementary Figure 1 Weight gain for C57BL/6J animals used for the proteomic analysis. Animals fed a diet high in fat (HFD) gained significantly more weight (a, p=0.004) than animals fed a 'standard fat diet' (SFD). *p<0.05; **p<0.01 *vs* SFD. n=5.

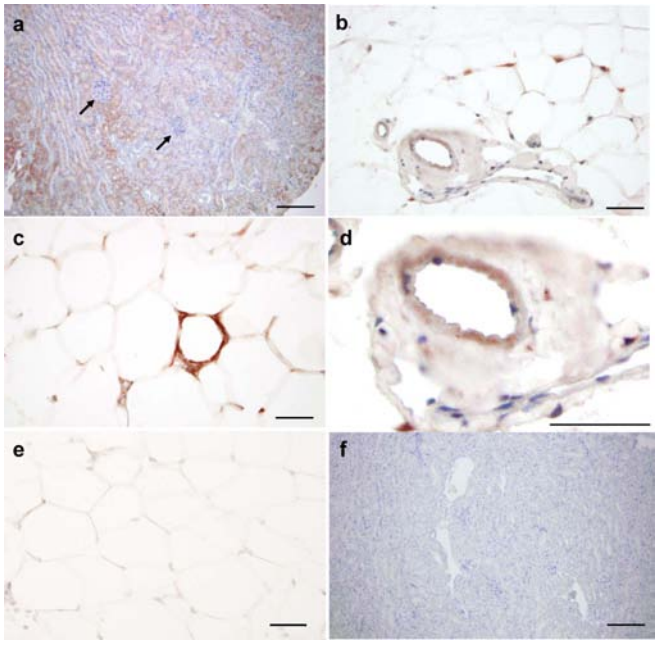

Supplementary Figure 2 Expression of sEH in adipose tissue. Kidney was used as a positive control. While most tubuli stained positive (a), glomeruli (arrows) lacked sEH as expected. In adipose tissue from lean (b, d) and obese (c) mice sEH expression was detected in endothelial cells (b, d), macrophages (c) and adipocytes (b,c). Endothelial cells were identified based on their presence in the blood vessel, while adipocytes and macrophages, organized in a typical crown-like structure, were distinguished based on their morphology. Adipose (e) and kidney (f) sections with omission of the anti-sEH IgG fraction did not show any detection. Bars for kidney and adipose sections are 200 and 50 μm, respectively. Nuclei are blue; sEH antigen is red.

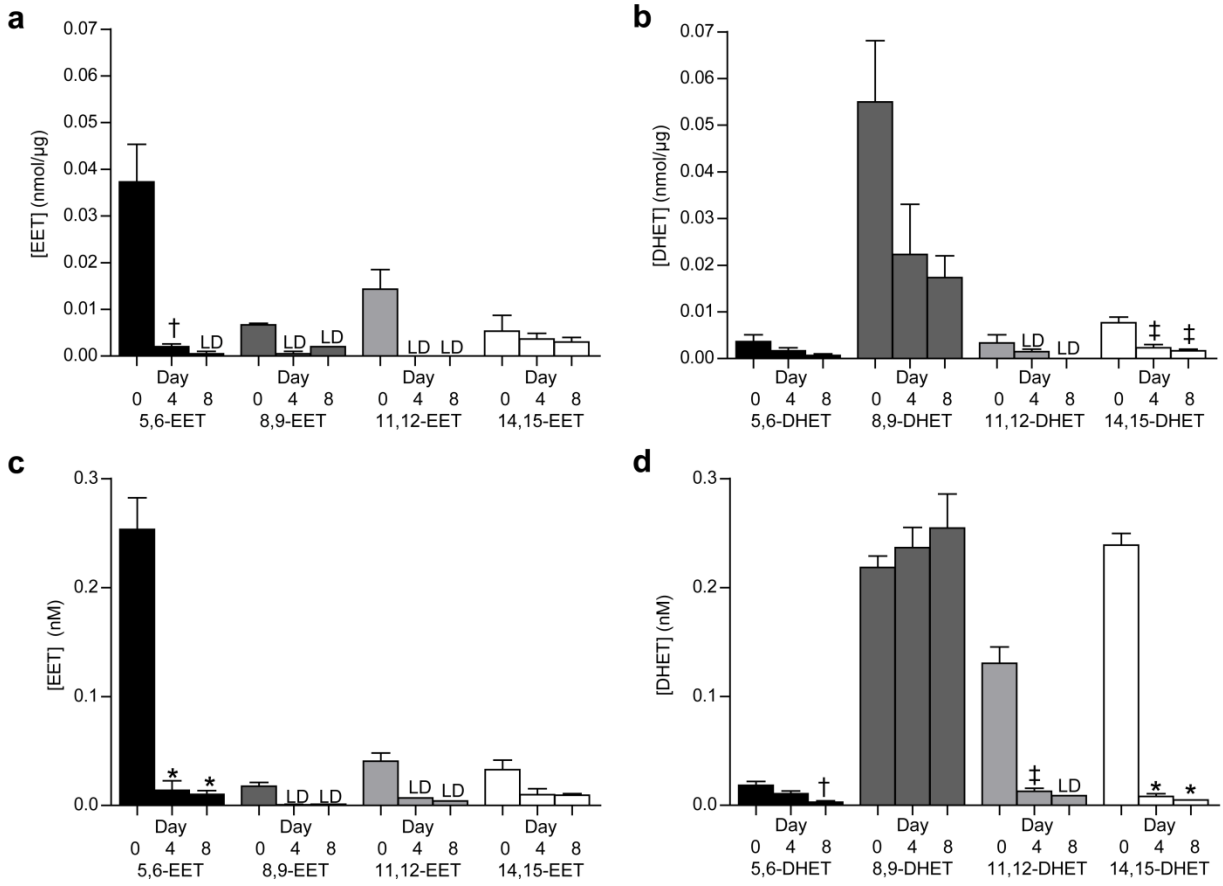

Supplementary Figure 3 EET (a, c) and DHET (b,d) levels in 3T3-L1 cells (a, b) and cell culture medium (c, d) during adipogenesis. EET and DHET levels are generally higher in the 3T3-L1 preadipocytes (day 0) than after 4 and 8 days of induction of differentiation. Levels at day 4 and 8 for some samples were below the level of detection (LD) (no statistical analysis possible). †$p<0.05$; ‡$p<0.01$; *$p<0.001$ *vs* day 0. n=3.

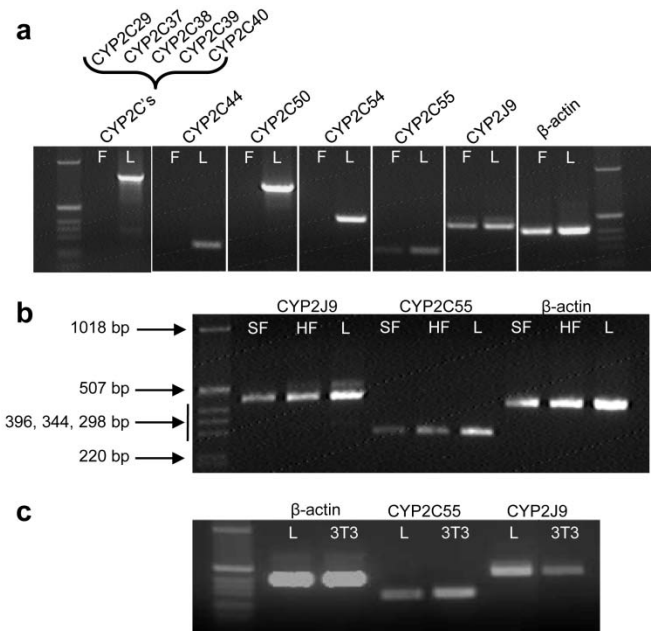

Supplementary Figure 4 EET producing CYP450 enzymes are expressed in adipose tissue and 3T3-L1 adipocytes. Using reverse transcriptase reactions for some different murine CYP450s known to produce EETs, it was shown that CYP2C55 and CYP2J9 were expressed in epididymal fat (F); liver (L) was used as a positive control (a). CYP2C primers recognize the different CYP2Cs and thus account for additional CYP2Cs in addition to those that were individually tested. CYP2C55 was not amplified by these primers potentially due to a lower reaction efficiency. CYP2J9 and CYP2C55 were expressed both in epididymal fat of mice fed regular chow (SF) and the 'western diet' (HF) (b). Finally, also in 3T3-L1 adipocytes CYP2C55 and CYP2J9 were expressed (c). The same DNA marker was used for a, b and c.

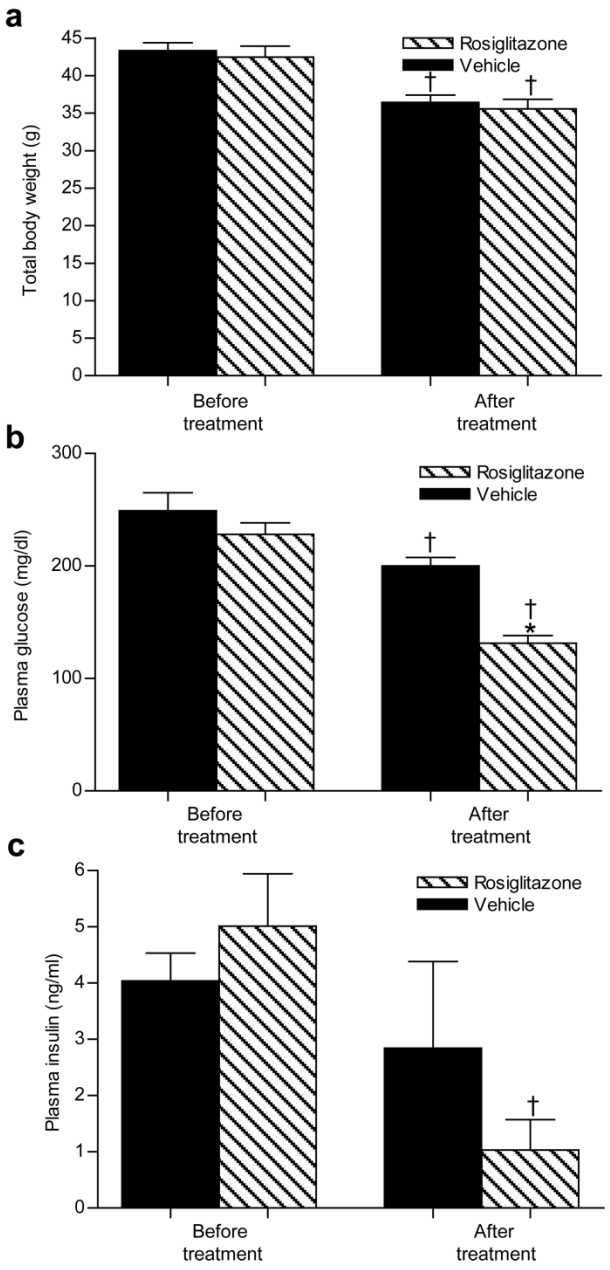

Supplementary Figure 5 Characterization of C57BL/6J animals used for treatment with rosiglitazone. While gavaging of mice generally resulted in weight loss, rosiglitazone itself did not influence weight (a). Rosiglitazone treatment reduced plasma glucose levels (b) and plasma insulin levels (c) determined after a 6 hour fasting period. †$p<0.05$ *vs* before treatment; *$p<0.05$ *vs* vehicle. n=5.

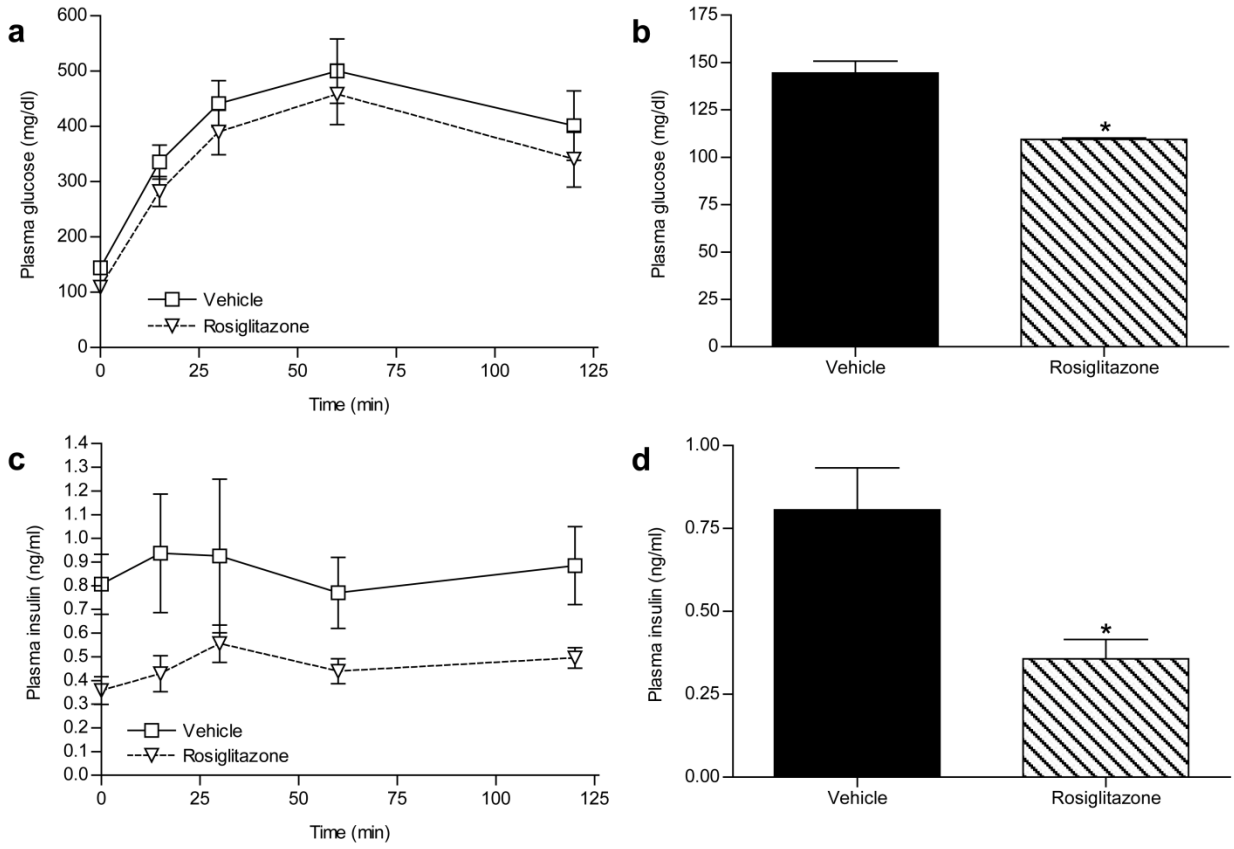

Supplementary Figure 6 Intraperitoneal glucose tolerance test (IPGTT) after rosiglitazone *vs* vehicle treatment. While plasma glucose levels were lower after a 16 hour fasting period in the rosiglitazone treated animals (b), no difference was observed in overall plasma glucose levels during the IPGTT using two-way ANOVA (a). Rosiglitazone reduced plasma insulin levels after a 16 hour fast (d), while ANOVA did not reveal a difference for the insulin levels during the IPGTT (c). While the power of the study (n=5) is most likely too low to observe a significant difference for a and c, b and d clearly show that rosiglitazone exerted the expected effect. *$p<0.05$ *vs* vehicle. n=5.

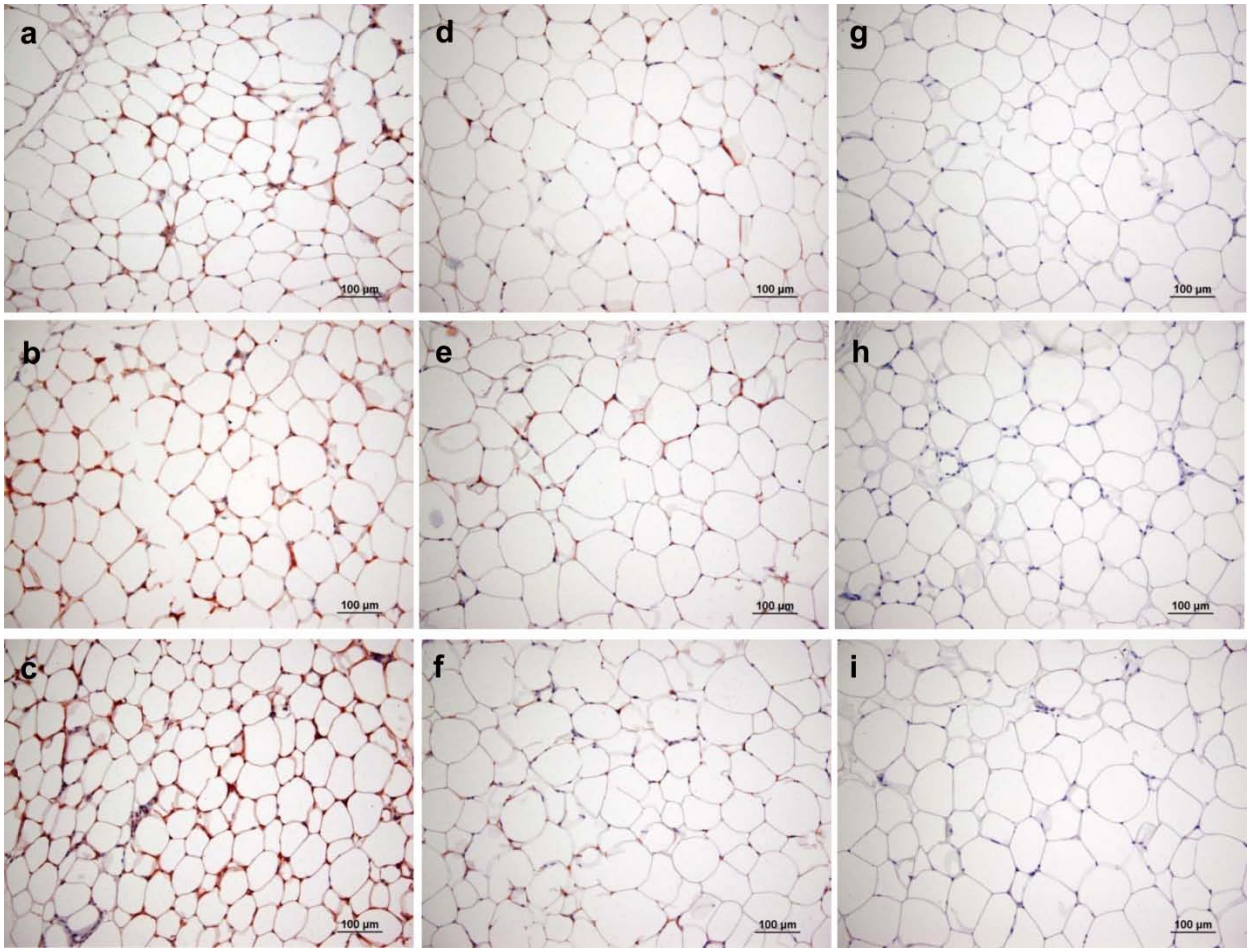

Supplementary Figure 7 Expression of sEH in epididymal adipose tissue of mice treated with rosiglitazone (a-c) *vs* vehicle (d-f). Adipose tissue sections with omission of the anti-sEH IgG fraction did not show any detection (g-i). Nuclei are blue; sEH antigen is red.